IEEE Access
Multidisciplinary | Rapid Review | Open Access Journal

Received 6 July 2022, accepted 22 July 2022, date of publication 26 July 2022, date of current version 29 July 2022.

Digital Object Identifier 10.1109/ACCESS.2022.3193998

RESEARCH ARTICLE

An SSM-PSO Based MPPT Scheme for Wind Driven DFIG System

BONI SATYA VARUN SAI[1], DEBASHIS CHATTERJEE[1], SAAD MEKHILEF[2,3,4], (Fellow, IEEE), AND ADDY WAHYUDIE[5,6], (Member, IEEE)

[1]Department of Electrical Engineering, Jadavpur University, Jadavpur, Kolkata 700032, India
[2]School of Science, Computing and Engineering Technologies, Swinburne University of Technology, Hawthorn, VIC 3122, Australia
[3]Center of Research Excellence in Renewable Energy and Power Systems, Smart Grids Research Group, King Abdulaziz University, Jeddah 21589, Saudi Arabia
[4]Department of Electrical Engineering, College of Engineering, Universiti Tenaga Nasional, Kajang, Selangor 43000, Malaysia
[5]Department of Electrical Engineering, United Arab Emirates University, Al Ain, United Arab Emirates
[6]National Water and Energy Center (NWEC), UAE-U, Al Ain, United Arab Emirates

Corresponding author: Boni Satya Varun Sai (satyavarunsai1234@gmail.com)

This work was supported by the Universiti Tenaga Nasional under the BOLD2025 Program through the Highly Cited Researchers (HCR) under Grant IC6-BOLDREFRESH2025.

ABSTRACT In this work, a searching space minimization-based particle swarm optimization (SSM-PSO) scheme has been proposed for maximum power point tracking (MPPT) in a doubly fed induction generator (DFIG) based wind energy conversion system (WECS). DFIG displays non-linearity in $P-\omega$characteristics. So different types of conventional and optimization-based schemes are developed for MPPT. The drawbacks in the conventional perturb and observe (P&O) scheme has been successfully abolished by the proposed SSM-PSO method. Because of its weather-insensitive nature, the conventional P&O MPP tracking scheme results in the fluctuation of DFIG output under a sudden change in wind speed. To avoid this problem, maximum and minimum limits for the optimal rotor speed have been determined in the proposed SSM-PSO scheme. Further, the obtained limits for rotor speed are employed to improve the searching space within the non-linear $P-\omega$ curve. This initial confinement of particles to a limited searching space in SSM-PSO results in a faster response of the system. Since the proposed SSM-PSO is atmosphere sensitive, it avoids fluctuations under an abrupt variation in wind velocity. The improved initialization part of SSM-PSO leads to better dynamic characteristics compared to existing P&O and optimization-based schemes. The proposed SSM-PSO scheme is implemented for a 2MW DFIG system in MATLAB Simulink atmosphere and showed satisfactory results.

INDEX TERMS Wind turbine, DFIG and maximum power point tracking.

I. INTRODUCTION

In the modern world, most of the consumed power is produced from non-renewable energy sources. Majority of these resources took ages to form from the organic carbon material, a major portion of the resources already has been exhausted [1]. More extraction of fossil fuels in meeting the exponentially rising load demand proves to be hazardous and uneconomical. If the usage of non-renewable sources continues at the present rate, there is a huge chance for complete exploitation by the end of 21st century. Therefore, the renewable energy sources like photovoltaic energy, wind power, etc., are came into the picture to counter the issue of power deficiency in the future. Wind power is most promising because of its abundant accessibility and pollution less nature compared to the other available renewable sources. The usage of wind energy for the residential purpose, leads to energy independence [2].

Irrespective of the size, the energy-producing wind turbine system contains different sections; they are the portion experiencing the wind force, tower, speed controlling apparatus and electrical generator. Generally, for WECS, any of the fixed or variable speed turbines are employed [3]. Due to its flexibility in operating at above-rated speeds,

The associate editor coordinating the review of this manuscript and approving it for publication was Akin Tascikaraoglu.

doubly fed induction generator (DFIG) is mostly considered for wind power generation. Moreover, DFIG has the advantages of variable speed and constant frequency operation, low mechanical tension, maximum power capturing ability, decoupled active or reactive power governance, etc. Also, the expenditure required for static power converters in DFIG is lower than that of permanent magnet synchronous generator (PMSG) [4]. These advantages in DFIG are due to the control schemes used in the back-to-back converters. Therefore, the process used in controlling back-to-back converters proves to display a vital role for the operating characteristics in DFIG. Because of its flexibility in the real power and reactive power decoupled control, vector control strategy is frequently employed in DFIG systems [5].

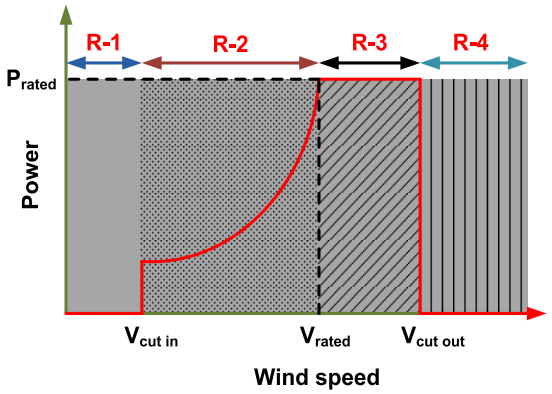

FIGURE 1. Different operating areas for wind turbine.

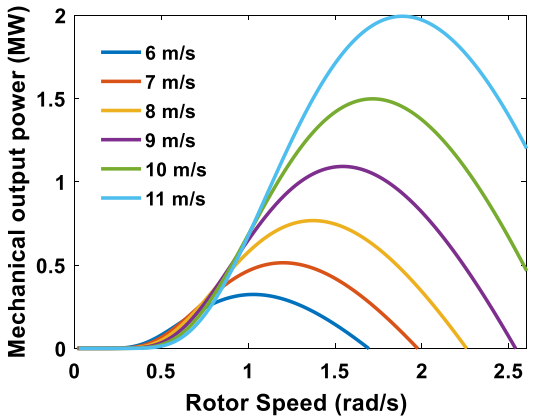

FIGURE 2. Power-speed characteristics at various wind speeds.

The working range for variable speed WECS is primarily divided into four regions, Region-1 (R-1), R-2, R-3, and R-4, as represented in Fig. 1. In R-1 and R-4, DFIG is not in the operating state, owing to safety measurements. In R-2, DFIG operates in MPP tracking zone, where the system is operated under below rated speeds. In R-3, DFIG operates in pitch controlling region, where the pitch controller is employed to reduce the stress over the wind turbines for above rated speeds [6]. As shown in Fig. 2, DFIG displays non-linear mechanical power and rotor speed characteristics. So, in DFIG, MPPT methods are employed for the efficient operation of the system. In MPP tracking, Perturb and Observe (P&O) scheme is considered to be prevalent because of its easy structure and flexible real-time operation. But, P&O displays fluctuation in output power characteristics under variation in speed situations and fails to track maximum power efficiently. P&O scheme operates with a small step and large step changes in rotor speed, where small step-change results in more settling time and less steady-state error [7]. With large steps, operation in P&O results in less settling time but more oscillation over a steady state. Many optimization-based schemes have already been available for tracking maximum power with improved dynamic characteristics compared to the P&O scheme.

A novel Robust Perturbation Observer based Fractional Order Sliding Mode Controller (RPO-FOSMC) has been proposed for tracking peak power [8]. RPO-FOSMC can display the improved dynamics compared to conventional MPPT schemes but results in the fluctuations of output power under a sudden change in speed cases. In [9], four sectors operation-based P&O scheme is implemented for faster tracking of peak power. The [9], displays a faster tracking response but undergoes more settling time compared to the large step P&O scheme. In [10], a fixed-time control scheme is used for MPP tracking in the DFIG system. In this method, aerodynamic torque is estimated without employing speed sensors with the help of a fixed-time observer. The Grouped grey wolf optimizer (GGWO) is employed to detect MPPT and improving fault ride-through capability for DFIG [11]. But the work should be expanded in grid side controller (GSC) side to operate the GGWO with the entire DFIG system.

An artificial Neural Network Controller (ANNC) assisted mechanical speed control is employed with a robust MPPT controller for studying wind power generation with respect to wind disturbances [12]. The novel fuzzy logic sensorless maximum power point tracking (FLC-MPPT) method for WECS is implemented by downsizing the pulse width modulation (PWM) back to back converters compared to conventional schemes by 40% [13]. Quantum parallel multi-layer Monte Carlo optimization algorithm, Archimedes optimization algorithm and Techno-economic optimization-based schemes are the few recently introduced optimization schemes in tracking maximum power [14]–[16]. A nonlinear maximum power point tracking scheme is introduced where the adaptive backstepping control method is employed for stable operation at speed disturbances and parametric uncertainties [17]. Estimation based enhanced maximum energy extraction scheme has been introduced for the MPPT case in DFIG, where it possesses the major advantage of easy real-time implementation [18]. For a DC-based DFIG system, MPPT is done by employing a coordinated adaptive feedback linearization controller (FLC-A) based on a flux observer [19].

Even though optimization-based schemes display better-operating characteristics, the settling time is longer.

Particle swarm optimization (PSO) is simpler to implement in real-time atmosphere due to its less mathematical formulation [20]. PSO and cuckoo search (CS) algorithms are the most commonly used approaches for MPPT in wind and PV generation [21]–[23]. Even though CS shows -operating properties than PSO, the latter is simpler while coming to real-time implementation [24]. Even though PSO is simpler, the development has to be done regarding the limitation of searching space, leading to lower settling time [25].

In this paper, an SSM-PSO scheme has been proposed as a modified version of the PSO scheme. The anemometer is used for tracking MPP in proposed scheme like [9], [28], [29]. The speed sensor is employed to minimize the searching space area, leading to improved dynamic characteristics and better accuracy. The proposed SSM-PSO scheme has been implemented for a 2MW DFIG-wind system in MATLAB-Simulink atmosphere. The proposed scheme is able to address the drawbacks of existing schemes and the major outcomes of SSM-PSO method are,

- Provides lower settling time compared to existing SS-P&O scheme.
- Results in lower steady state oscillations compared to existing LS-P&O scheme.
- Under sudden change in wind speeds, proposed SSM-PSO displays lower oscillations in output characteristics compared to LS and SS P&O schemes.
- The proposed scheme is flexible and can be easily implemented with existing drive-compatible hardware.

This paper is articulated as System Configuration in section 2, Control Strategies in DFIG system in section 3, Proposed SSM-PSO based MPPT for DFIG in section 4, Simulation Results and Discussions in section 5, and Conclusion in section 6.

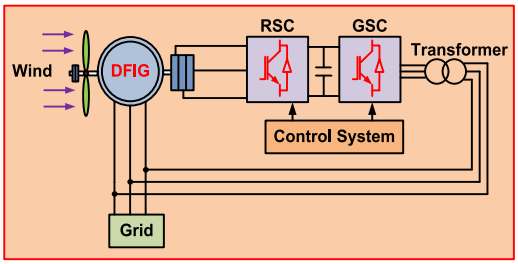

FIGURE 3. Schematic circuit for DFIG system.

II. SYSTEM CONFIGURATION

The wind-turbine-based DFIG system transforms wind power into electrical power. Fig. 3, displays the block diagram for a 2 MW DFIG system, where the energy is transferred over a direct connection and back-to-back converter topology to the grid. The grid side converter (GSC) controlling has a major purpose of maintaining a constant DC-link voltage in the proposed topology, irrespective of the direction and quantity of the rotor power. The independent controlling of reactive power and rotor speed is the major objective of the rotor side controller. As the proposed work is more related to MPPT, only Rotor side converter (RSC) controller design is considered in the present research work, as displayed in Fig. 4. In the proposed scheme, the estimation of the rotor position and speed is done by employing the model reference adaptive system (MRAS) control technique [27].

TABLE 1. System parameters.

Wind turbine	
Number of blades	3
Gear Ratio (N)	100
Blade radius (R)	42 m
Air density (ρ)	1.225 kg/m^3
Optimal Tip speed ration (λ_{opt})	7.2
Maximum power coefficient (C_{p_max})	0.44
Unknown coefficients (C_1-C_7)	C_1=0.73, C_2=151, C_3=0.58, C_4=0.002 C_5=2.14, C_6=13.2, C_7=-18.4
DFIG parameters	
Peak power	2 MW
Pole pair (p)	2
Rated torque	12.7 K-Nm
Stator connection	Star
Stator resistance (R_s)	2.6 $m\Omega$
Stator leakage inductance $(L_{\sigma s})$	87 μH
Magnetizing inductance (L_m)	2.5 mH
Turns ratio (u)	0.34
Rotor resistance (R_r)	26.1 $m\Omega$
Rotor leakage inductance $(L_{\sigma r})$	783 μH
Rated stator voltage (V_s)	690 V_{rms}
Rated stator current (i_s)	1760 A_{rms}
Rated rotor voltage (V_r)	2070 V_{rms}
Stator inductance (L_s)	2.587 mH
Rotor inductance (L_r)	2.587 mH

A. WIND TURBINE MODELLING

The mechanical power developed in the wind turbine is represented as (1), where β is pitch angle, ρ is air density (kg/m^3), C_p is power coefficient of a wind turbine, A is the swept area (m^2), V_w is wind velocity(m/sec), and λ is tip speed ratio. The C_p is calculated using (2), where C_1 to C_7 values are as represented in Table-1. From (2), λ_i is calculated in terms of β and λ as (3). For a known value of wind speed, λ is calculated as a function of rotor speed (ω_m) as shown in (4). At the optimum power case, (4) can be formulated as (5).

$$P_m = \frac{1}{2}\rho A C_p(\beta, \lambda) V_w^3 \tag{1}$$

$$C_p = C_1\left(\frac{C_2}{\lambda_i} - C_3\beta - C_4\beta^{C_5} - C_6\right)\left(e^{C_7/\lambda_i}\right) \tag{2}$$

$$\lambda_i = \frac{1}{\lambda + 0.02\beta} - \frac{0.003}{1+\beta^3} \tag{3}$$

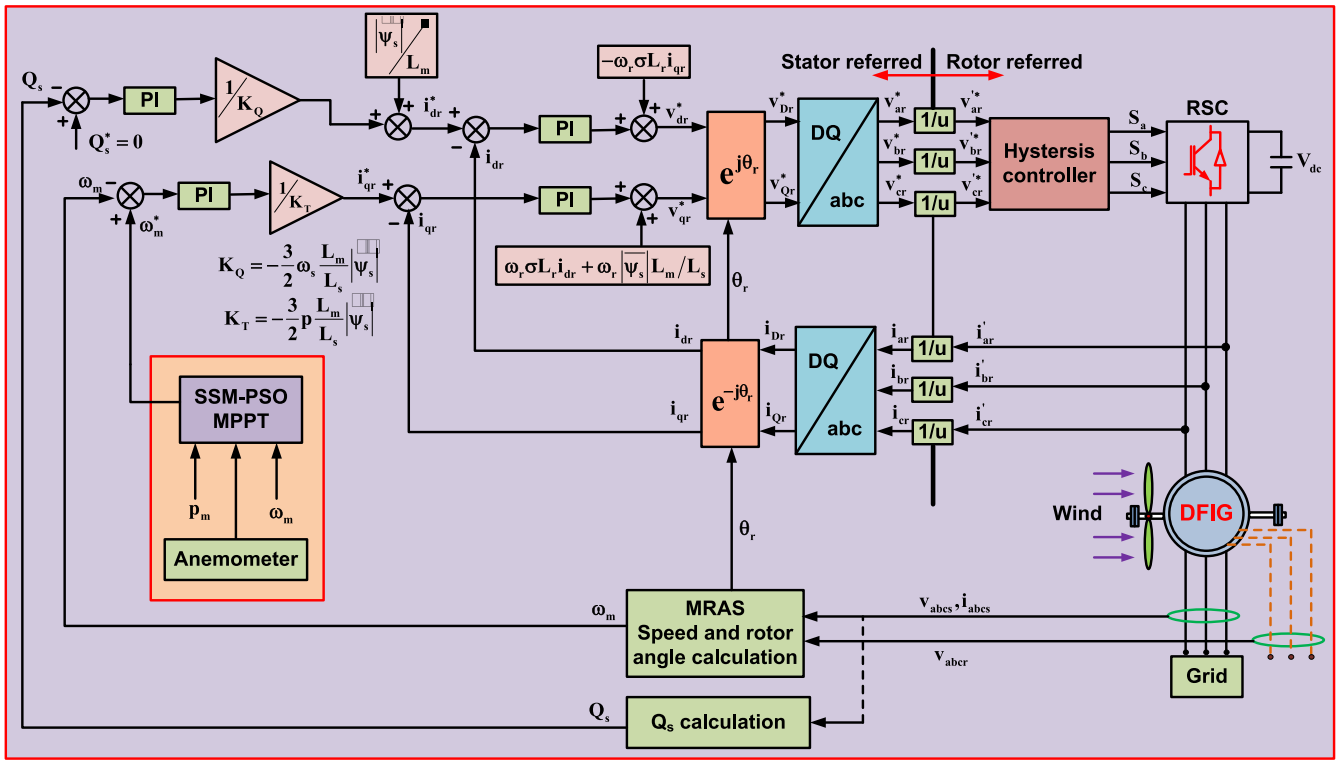

FIGURE 4. The control scheme for the proposed system.

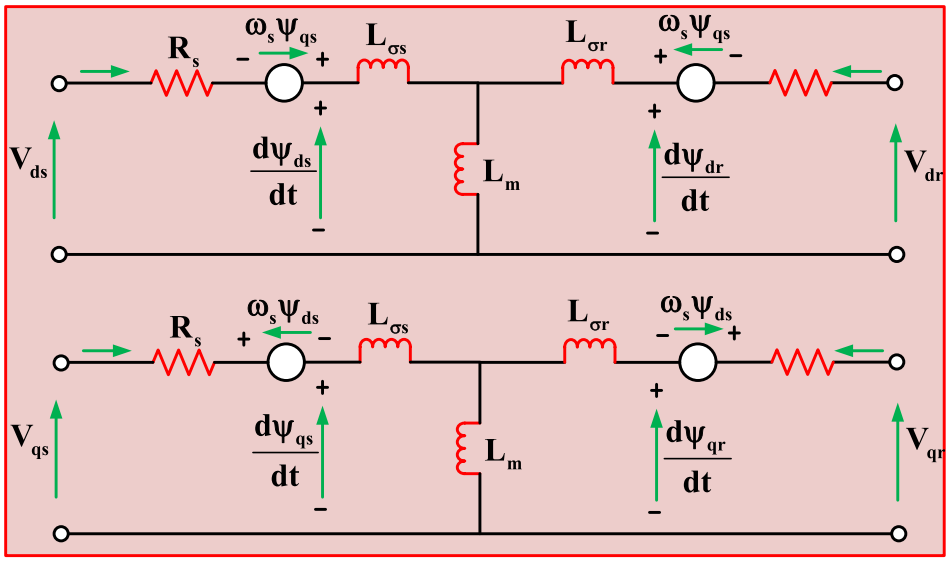

FIGURE 5. DFIG modelling in dq-reference frame.

$$\lambda = \frac{\omega_m R}{V_w} \tag{4}$$

$$\lambda_{opt} = \frac{\omega_{opt} R}{V_w} \tag{5}$$

B. DFIG MODELLING

In Fig.5, DFIG modelling using a dq-reference frame is represented. The equations for stator and rotor voltages in dq components are represented in (6)-(9), where V_{ds}, V_{qs}, V_{dr} and V_{qr} are dq components of stator voltages and rotor voltages, ψ_{ds}, ψ_{qs}, ψ_{dr} and ψ_{qr} are dq components of stator flux and rotor flux, i_r is rotor current, ω_r is rotor speed, ω_s is synchronous speed, i_{ds}, i_{qs}, i_{dr} and i_{qr} are dq components of stator and rotor currents, ψ_s is stator flux and ψ_r is rotor flux.

$$v_{ds} = R_s i_{ds} + \frac{d\psi_{ds}}{dt} - \omega_s \psi_{ds} \tag{6}$$

$$v_{qs} = R_s i_{qs} + \frac{d\psi_{qs}}{dt} - \omega_s \psi_{qs} \tag{7}$$

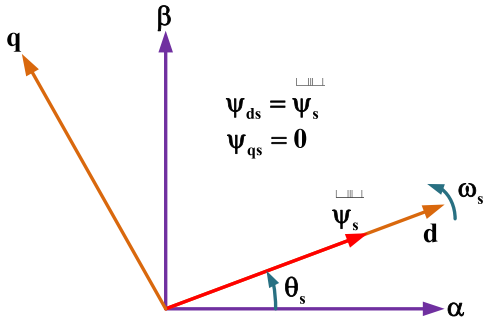

FIGURE 6. The stator flux space vector alignment with synchronous rotating dq frame.

$$v_{dr} = R_r i_{dr} + \frac{d\psi_{dr}}{dt} - \omega_r \psi_{dr} \tag{8}$$

$$v_{qr} = R_r i_{qr} + \frac{d\psi_{qr}}{dt} - \omega_r \psi_{qr} \tag{9}$$

In the same manner, the flux developed in DFIG system are represented using (10)-(13).

$$\psi_{ds} = L_s i_{ds} + L_m i_{dr} \tag{10}$$

$$\psi_{qs} = L_s i_{qs} + L_m i_{qr} \tag{11}$$

$$\psi_{dr} = L_m i_{ds} + L_r i_{dr} \tag{12}$$

$$\psi_{qr} = L_m i_{qs} + L_r i_{qr} \tag{13}$$

where the electromagnetic torque T_{em} is represented as,

$$T_{em} = \frac{3}{2} p \frac{L_m}{L_s} \left(\psi_{qs} i_{dr} - \psi_{ds} i_{qr}\right) \tag{14}$$

III. CONTROL STRATEGIES IN THE DFIG SYSTEM

Since the proposed scheme focuses mainly on maximum power point tracking, RSC controlling is mainly discussed in this paper compared to GSC controlling. While, in the proposed scheme, the DC-link voltage is voltage is maintained constant by employing the scheme same as [11] at GSC.

A. ROTOR CURRENT CONTROL LOOPS

Out of available controlling schemes in DFIG, the proposed system has been operated with the vector control. The control structure has been explained in steps for better understanding, where the first step is about examining the current loops. As shown in Fig. 6, vector control is performed in a synchronous revolving dq frame, where the stator flux is aligned with the dq frame [1]. Due to this, it can be represented that the rotor current and torque or active stator power are proportional to the reactive power and quadrature rotor current, respectively.

$$v_{dr} = R_r i_{dr} + \sigma L_r \frac{di_{dr}}{dt} - \omega_r \sigma L_r i_{qr} + \frac{L_m}{L_s} \frac{d\left|\vec{\psi_s}\right|}{dt} \tag{15}$$

$$v_{qr} = R_r i_{qr} + \sigma L_r \frac{di_{qr}}{dt} + \omega_r \sigma L_r i_{dr} + \omega_r \frac{d\left|\vec{\psi_s}\right|}{dt} \tag{16}$$

By substituting (10)-(13) in (6)-(9), rotor voltage can be represented in terms of stator flux (note that $\psi_{qs} = 0$) and rotor currents (15)-(16). In (15) and (16), leakage factor, $\sigma = 1 - L_m/L_s \cdot L_r$. Since, the grid and stator are directly connected, stator flux is considered to be constant $\left\{\left(d\left|\vec{\psi_s}\right|/dt\right) = 0\right\}$ in (15) and (16). From (15) and (16), it can be noted that d-q rotor currents can be controlled by simply employing the PI controller for individual current components, as shown in Fig. 4. If DFIG displays a different stator to rotor turns ratio, it should be employed in the control scheme. The current reference values in Fig. 4, are generated with speed and power control loops. In Fig. 4, stator side referred rotor currents are employed in current loops working, while the rotor-referred quantities conversion is executed at the currents and before the creation of the pulses for the converter for the voltages. The corresponding closed-loop transfer function displays a second-order system with one zero, where the appropriate gain values for the PI controller can be designed using classic control theory [1].

B. SPEED AND POWER CONTROL LOOPS

Since the stator flux space vector is in phase with the d-axis in the reference frame, (14) can be modified as,

$$T_{em} = -\frac{3}{2} p \frac{L_m}{L_s} \left|\vec{\psi_s}\right| i_{qr} \approx K_T i_{qr} \tag{17}$$

From (17), it can be observed that, electromagnetic torque is proportional to the q-axis rotor current. Therefore, electromagnetic torque can be controlled by employing rotor current. Also, it can be used in controlling the speed of the DFIG, if the application needs it. From (18), it can be noted that, the d-axis rotor current has its effect on stator reactive power.

Therefore, from the axis orientation employed, it can be observed that the dq components of rotor currents can be employed in controlling reactive power and torque autonomously. The same has been employed in the complete control scheme, as shown in Fig. 4. In Fig. 4, speed and power control loops are employed for the overall controlling scheme along with current controlling loops. Moreover, by using Q_s loop, the magnetization of the machine can be controlled. The magnitude of stator flux is considered to be constant, as the grid and stator are directly associated, and can be calculated by employing grid voltage. The stator flux equations can be represented as (19).

$$\left.\begin{aligned} Q_s &= \frac{3}{2}\left(v_{qs} i_{ds} - v_{ds} i_{qs}\right) \\ Q_s &= -\frac{3}{2}\omega_s \frac{L_m}{L_s}\left|\vec{\psi_s}\right|\left[i_{dr} - \frac{\left|\vec{\psi_s}\right|}{L_m}\right] \\ Q_s &= K_Q\left[i_{dr} - \frac{\left|\vec{\psi_s}\right|}{L_m}\right] \end{aligned}\right\} \tag{18}$$

$$\left|\vec{\psi_s}\right| = \psi_{ds} = L_s i_{ds} + L_m i_{dr}, \quad \psi_{qs} = 0 = L_s i_{qs} + L_m i_{qr} \tag{19}$$

For real-time applications, different Q_s values are required based on grid codes. Thus, the grid system operator can set the

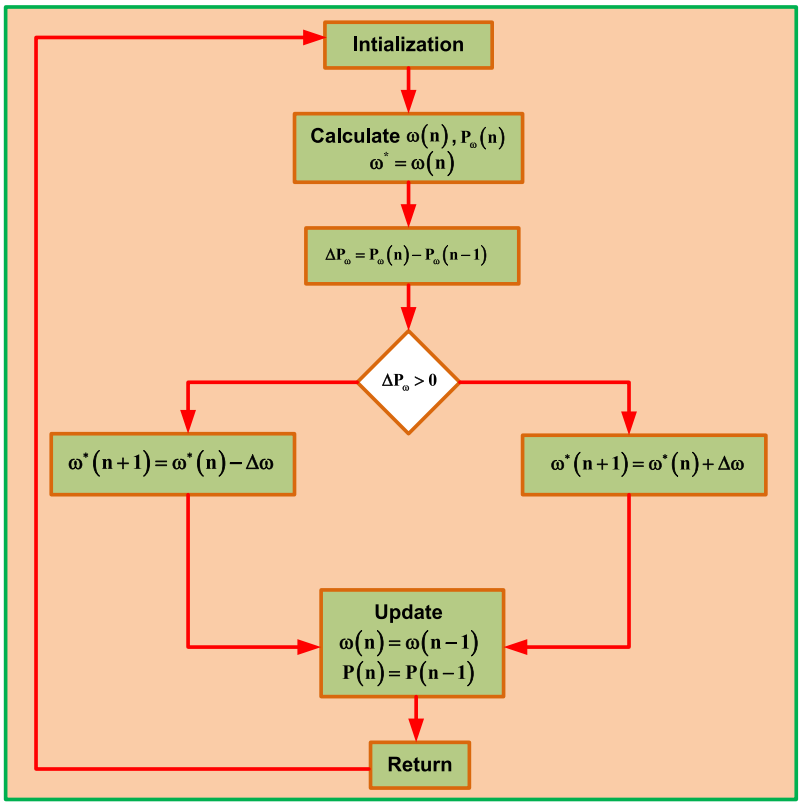

FIGURE 7. Perturb and observe MPPT scheme.

Q_s reference directly. From Fig. 4, it is assumed that internal current control loops execute faster than the external speed and power control loops to avoid the computation delay. The speed and power control loops can be modeled as first and second-order systems, where the tuning is done to fix the PI controller gain values. The proposed scheme generates the speed reference by the SSM-PSO technique for tracking maximum power. Fig. 4 represents the overall vector scheme with proposed SSM-PSO scheme, where the system results in constant torque at varying speed. The stator voltage can be assumed constant because of the direct linkage between stator and grid. As T_{em} and Q_s are constants, the stator currents are also maintained at constant values.

IV. THE PROPOSED SSM-PSO BASED MPPT FOR DFIG

The P&O method is widely employed to track MPP for WECS [7]. Fig. 7, represents the flowchart for existing P&O, where the sensed mechanical power (P_m) and rotor speed (ω) are used for tracking maximum power [9]. The P&O scheme operates in two types of steps they are, large steps (LS) and small steps (SS). The larger step change in rotor speed ($\Delta\omega$) value in the P&O scheme results in the faster system response, but it results in the large fluctuations over the steady-state operation. Moreover, due to its weather-insensitive nature, the P&O scheme displays higher fluctuations in the output characteristics under an abrupt variation in wind speed. P&O scheme with a smaller $\Delta\omega$ value results in the slower response, but it results in lower fluctuations over the steady-state operation. Moreover, the smaller step value results in the lower efficiency during maximum power point (MPP) tracking.

PSO is most famously utilized advancement framework for discovering global maximum under non-linear operation. PSO has been modelled based on bird flock's behavior, it is a speculative and population-based evolutionary algorithm (EA) search technique. A Swarm of individuals is maintained by the PSO algorithm in which each particle signifies a candidate solution. Particles track a basic conduct in which they mime the accomplishment of neighboring particles and their own accomplished victories. Therefore, best particle (P_{best}) in neighborhood affects the particle's position, along with the best solution (G_{best}) discovered by the particle itself. Particle location, x_i, is updated by employing [24],

$$x_i^{k+1} = x_i^k + v_i^{k+1} \tag{20}$$

where step size is represented by velocity component, v_i. The velocity is formulated by,

$$v_i^{k+1} = \omega v_i^k + c_1 r_1 \left\{ P_{besti} - x_i^k \right\} + c_2\, r_2 \left\{ G_{best} - x_i^k \right\} \tag{21}$$

where random numbers $r_1, r_2 \in u\,(0, 1)$, c_1 and c_2 are coefficient of acceleration and ω is inertia weight. The personal best position of particle i is P_{besti} and the best position of

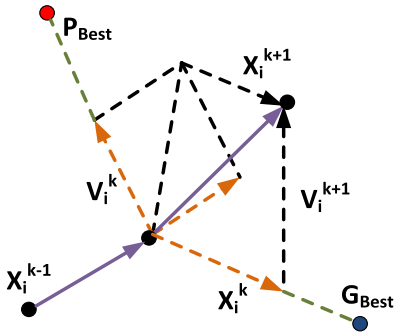

FIGURE 8. Particle movement in particle swarm optimization.

the particles is G_{best}. In Fig. 8, the particles in optimization practice with distinctive movement are represented. If the original rotor speed defines the position, then rotor speed perturbation is displayed by the velocity. Therefore, (20) is further formulated as,

$$\omega_i^{k+1} = \omega_i^k + v_i^{k+1} \tag{22}$$

From Fig. 7 and (22), it can be observed that, the overall operating structure in the P&O scheme and PSO scheme are similar. But, in PSO perturbation in present, the rotor speed is based on the P_{besti} and G_{best}. If the rotor speed is nowhere near the other two rotor speeds, then the subsequent variation in rotor speed is higher and vice-versa. In P&O, perturbation in rotor speed is constant, while in PSO, the perturbation varies with position of the particles.

A. SSM-PSO FORMULATION IN DFIG MPPT

Before describing PSO implementation in MPP tracking, a solution vector of rotor speeds with Np particles has been considered as,

$$\begin{aligned} x_i^k &= \omega_g = \left[\omega_1, \omega_2, \omega_3, \ldots\ldots, \omega_j\right] \\ j &= 1, 2, 3, 4, \ldots\ldots\ldots\ldots\ldots\ldots N_P \end{aligned} \tag{23}$$

The objective function is formed with the idea of comparing the power of updated power with the former one as a function of rotor speed. So, the objective function can be defined as,

$$P\left(\omega_i^k\right) - P\left(\omega_i^{k-1}\right) = f_k \tag{24}$$

The function f_k can be calculated subjected to $P\left(\omega_i^k\right) > P\left(\omega_i^{k-1}\right)$, where $P(\omega_i)$ can be obtained using (1)-(4).

To initialize the optimization procedure, assume that the flowchart communicates three-rotor reference speeds, as shown in Fig. 4. In Fig. 9, three different rotor speeds ω_1, ω_2 and ω_3 are represented using square, circular and triangular notations, respectively. These rotor speeds are used as P_{besti} in the first iteration. Of these three particles, particle 2 is said to be G_{best}, as it can be noted that, particle 2 is nearer to the maximum power. In the second iteration, the resultant velocity is only because of the G_{best} parameter. Since, the

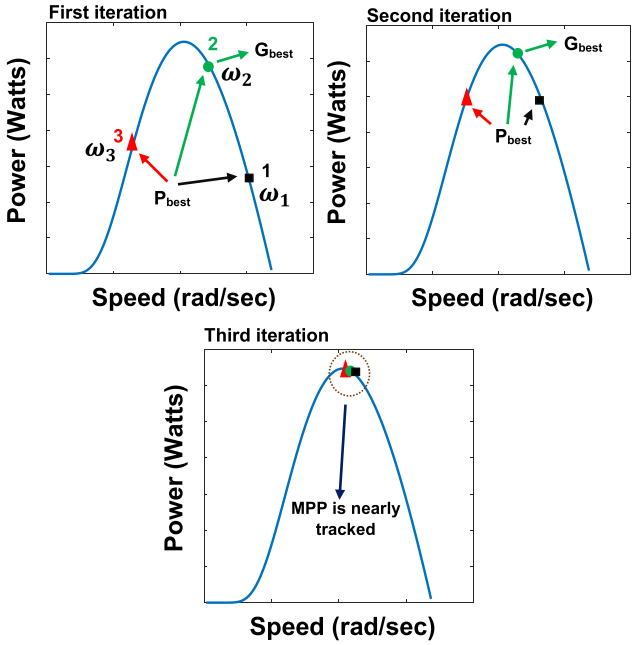

FIGURE 9. Particle movement for MPPT process in PSO scheme.

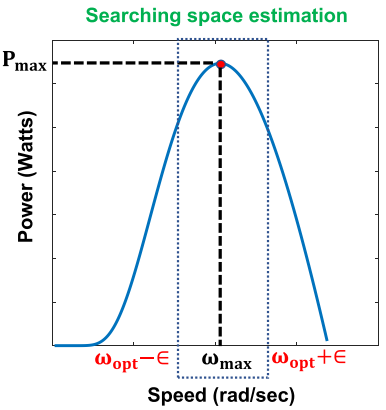

FIGURE 10. Searching space mechanism in the proposed system.

$(P_{besti} - \omega(2))$ is zero in (21), the velocity of G_{best} particle $(\omega(2))$ becomes zero. So, it can be observed that, the velocity of particles becomes zero and there is no use of this particle in further exploration of MPP.

To avoid this, perturbations in particles are allowed, as shown in the second iteration of Fig. 9. Since the previous rotor speeds in the system operate at better fitness values, the particles are driven towards G_{best} with low velocity [26]. In the third iteration of Fig. 9, it can be noted that all three particles arrive at an MPP. Due to the very low velocity, all three particles are arriving a constant value, avoiding the oscillation over steady-state, unlike P&O.

B. PROPOSED SSM-PSO FOR SEARCHING SPACE OPTIMIZATION

$$\omega_{opt} = \frac{\lambda_{opt} V_w}{R} \tag{25}$$

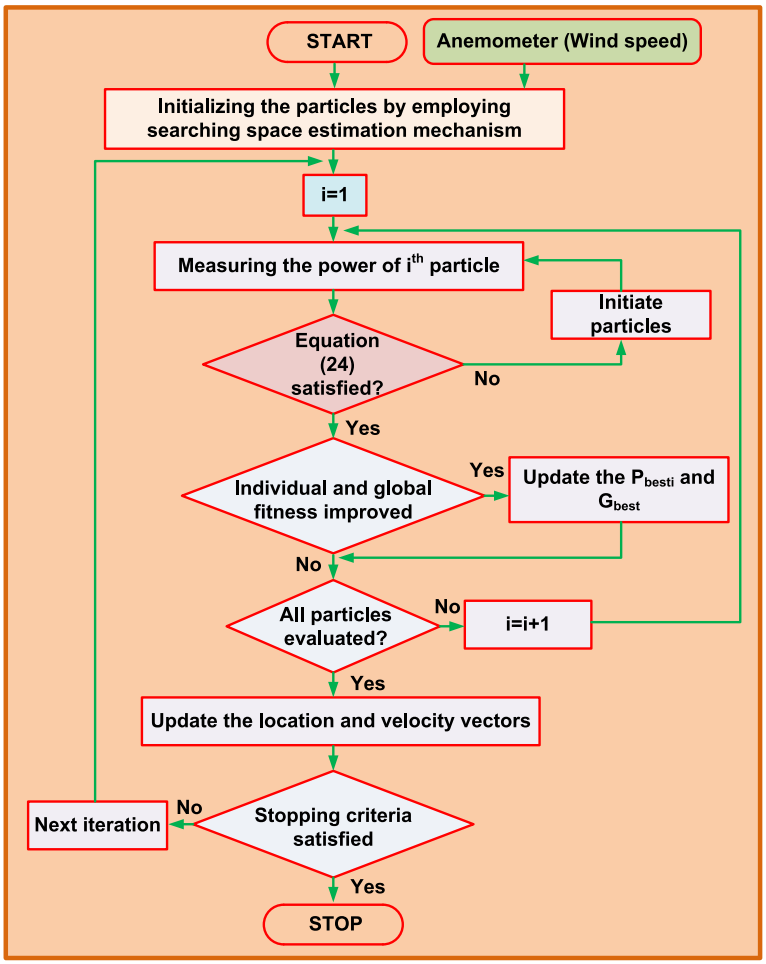

FIGURE 11. Proposed SSM-PSO algorithm.

In the proposed SSM-PSO, the actual improvement is made to reduce the searching space. Fig. 11, represents the proposed SSM-PSO mechanism for MPP tracking in DFIG. Using the anemometer, the optimum rotor speed value can be obtained using (25). The searching space can be minimized by employing a constant, as represented in Fig. 10. The particles at different positions are initialized using (26), where $\omega_{\max}$ and $\omega_{\min}$ are calculated using (27) and (28) in the proposed system.

$$x_i = \omega_{\min} + \frac{(i-1)\left[\omega_{\max} - \omega_{\min}\right]}{N_p - 1}$$
$$i = 1, 2, 3, 4, \ldots\ldots\ldots\ldots\ldots\ldots, N_p \quad (26)$$
$$\omega_{\max} = \omega_{opt} + \in \quad (27)$$
$$\omega_{\min} = \omega_{opt} - \in \quad (28)$$

By employing the searching space estimation mechanism, the particle's placement area over $P - \omega$ is minimized. The derived reference rotor speed from SSM-PSO has been compared with the actual rotor speed, as shown in Fig. 4, for tracking maximum power. The SSM-PSO results in better tracking efficiency and near-zero steady oscillations.

Moreover, the proposed SSM-PSO scheme displays better dynamic characteristics compared to the P&O scheme with a low step and large step operations. The searching space minimization mechanism used in proposed scheme is independent of generator type. It depends mainly on the wind speed, sensed by anemometer. So, SSM-PSO scheme can be implemented for the generators other than DFIG.

V. SIMULATION RESULTS AND DISCUSSIONS

The proposed SSM-PSO scheme has been simulated for a DFIG-Wind Turbine system in a MATLAB-simulink environment. The DFIG-wind system is implemented in MATLAB with design parameters as given in Table-1. The proposed scheme has been tested for step and random variations of wind speeds. Moreover, the existing LS-P&O and SS-P&O [7] schemes are compared with the proposed scheme for the same changes in the wind speed to prove the proposed scheme's usefulness.

A. SINGLE STEP VARIATIONS IN WIND SPEED

The proposed SSM-PSO, SS-P&O and LS-P&O are operated for a step-up variation in wind speed from 6 m/s to 8 m/s,

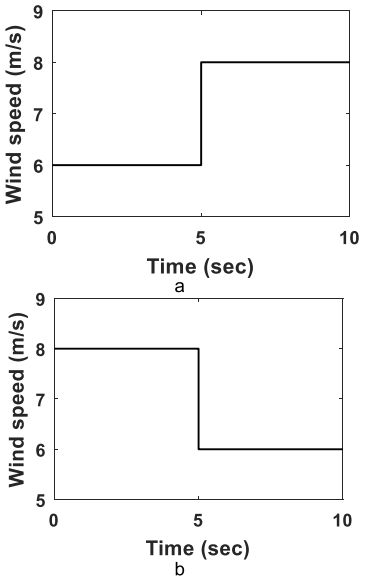

FIGURE 12. Single Step changes in wind-speed (a) Step-up (b) Step-down.

TABLE 2. Comparison of SSM-PSO with existing MPPT schemes.

Algorithms	Settling time	Oscillations	Efficiency
LS-P&O [7]	77 ms	1.2	--
SS-P&O [7]	>1300 ms	0.05	87.11%
MP&O [7]	930 ms	0.3	88.23%
RA-P&O [7]	<600 ms	0.001	91.39%
Proposed SSM-PSO	<350 ms	0.001	92.01%

as represented in Fig. 12a. The rotor side characteristics such as tip speed ratio, power coefficient, rotor speed and mechanical power are represented as shown in Fig. 13a, 13b, 13c and 13d, respectively.

Also, the proposed SSM-PSO, SS-P&O, and LS-P&O are operated for a step-down variation in wind speed from 8 m/s to 6 m/s, as represented in Fig. 12b. The rotor side characteristics with step-down variation are represented as shown in Fig. 14a, 14b, 14c, and 14d, respectively.

Overall, from Fig. 13 and 14, it can be observed that, the LS-P&O scheme settles faster compared to SS-P&O and SSM-PSO schemes. But it is noted that, LS-P&O exhibits higher oscillations over a steady-state, leads to the inefficiency of the system. Coming to LS-P&O, from Fig. 13 and 14, it is noted that, LS-P&O leads to lower steady-state oscillations. On the other hand, the LS-P&O has a major disadvantage of higher settling time or slower response. The proposed SSM-PSO scheme displays both the advantages of faster response and lower steady-state error.

From Fig. 13 and 14, it can be observed that, the settling time of LS-P&O is around 80 ms, for SS-P&O, settling time is around 1300 ms and finally, for proposed SSM-PSO, it is around 350ms. From Fig 13a and 14a, it can be observed

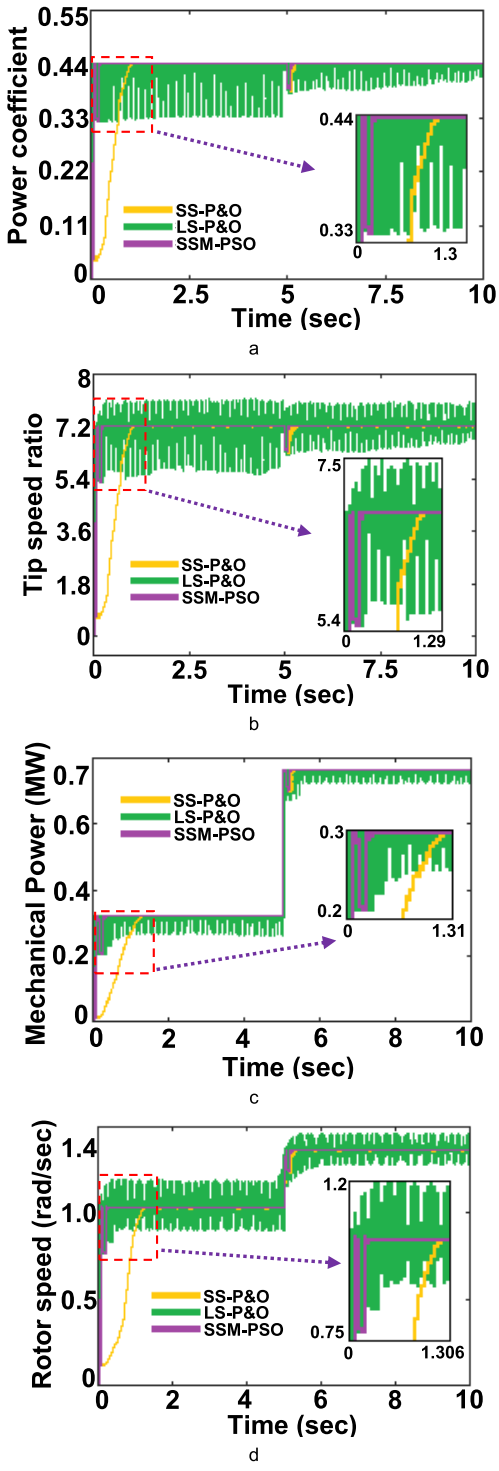

FIGURE 13. Rotor side characteristics for single step-up variation in wind speed (a) Power coefficient (b) Tip speed ratio (c) Mechanical power (d) Rotor speed.

that, the proposed SSM-PSO method preserves the C_{p_max} successfully related to LS-P&O and SS-P&O schemes. From 13c and 14c, it is noted that the proposed SSM-PSO method tracks the mechanical power efficiently related to LS-P&O and SS-P&O schemes. The comparison of tracked maximum

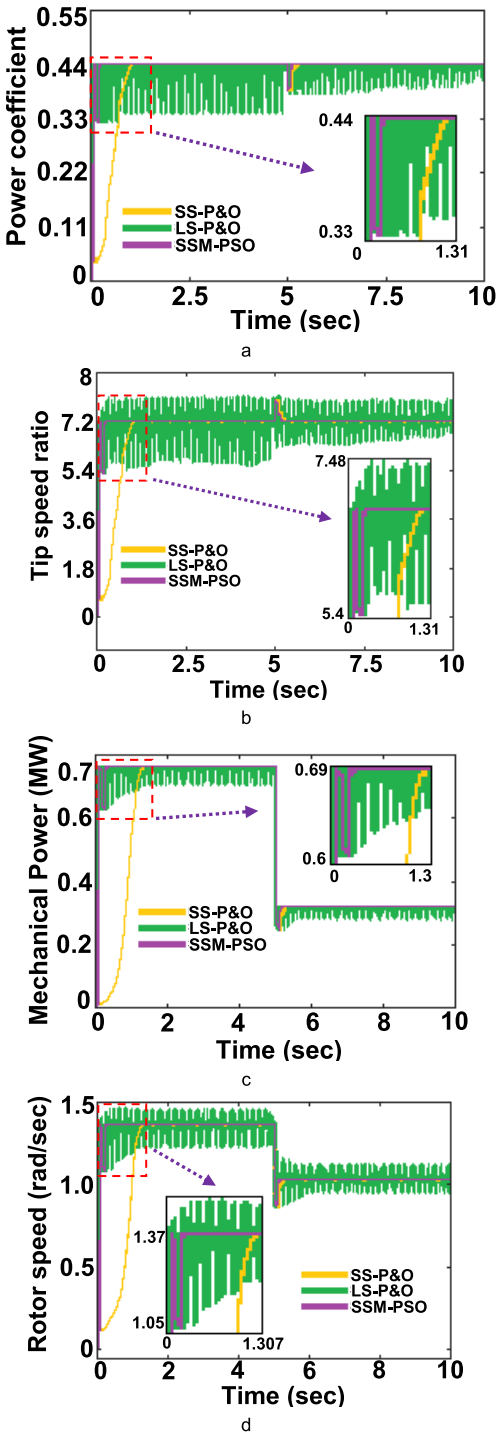

FIGURE 14. Rotor side characteristics for single step-down variation in wind speed (a) Power coefficient (b) Tip speed ratio (c) Mechanical power (d) Rotor speed.

power with actual maximum power at wind speeds of 6 m/s and 8 m/s are represented in Fig. 20. From, Fig. 13d and 14d, it is noted that, the peak to peak oscillation in LS-P&O is higher compared to SS-P&O and SSM-PSO schemes.

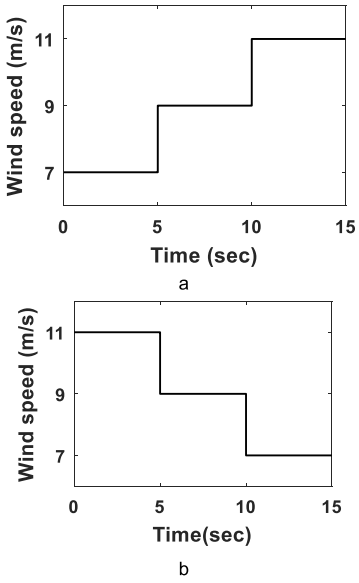

FIGURE 15. Two Step changes in wind-speed (a) Step-up (b) Step-down.

B. TWO-STEP VARIATIONS IN WIND SPEED

The proposed SSM-PSO SS-P&O and LS-P&O are operated for a two-step-up variation in wind velocity from 7 m/s to 9 m/s to 11 m/s as shown in Fig. 15a. The rotor side characteristics with two step-up variations in wind velocity are represented as shown in Fig. 16a, 16b, 16c and 16d, respectively.

As displayed in Fig. 15b, the proposed SSM-PSO, SS-P&O and LS-P&O are operated for a two-step-down variation in wind speed from 11 m/s to 9 m/s to 7 m/s. The rotor side characteristics with two-step-down variation are represented as shown in Fig. 17a, 17b, 17c and 17d, respectively.

From Fig. 16 and 17, it can be observed that the proposed SSM-PSO scheme displays better dynamic characteristics compared to LS-P&O and SS-P&O schemes under multiple wind speed step variations. Even in the sudden speed variations, the proposed scheme does not divert its tracking path and tracks the maximum power efficiency. The tracked power is related with the actual power in Fig. 20. From this, it is observed that the proposed SSM-PSO displays average efficiency of 92.01%.

C. RANDOM VARIATION IN WIND SPEED

The proposed SSM-PSO scheme has been operated for random wind speed variation, as shown in Fig. 18. The respective rotor side characteristics are represented in Fig. 19a, 19b, 19c & 19d, respectively. From Fig. 19, it is noted that the proposed SSM-PSO tracks maximum power more efficiently compared to LS-P&O and SS-P&O. Moreover, due to its weather-sensitive nature, the SSM-PSO displays no drift under variation of wind speed along with near-zero steady-state oscillation.

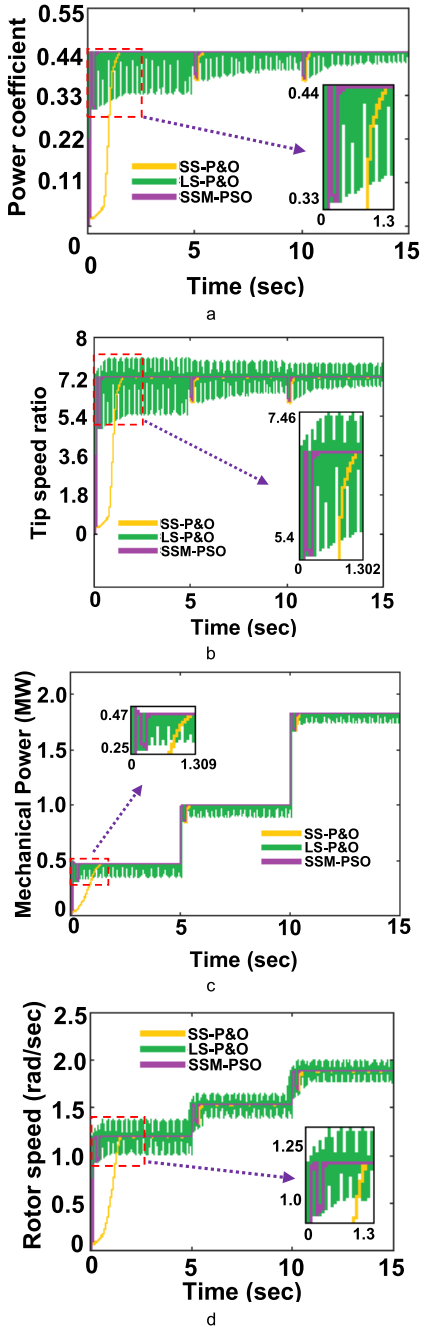

FIGURE 16. Rotor side characteristics for two step-up variation in wind speed (a) Power coefficient (b) Tip speed ratio (c) Mechanical power (d) Rotor speed.

D. OVERALL COMPARISON BETWEEN SSM-P&O AND EXISTING MPPT SCHEMES

To justify the advantage of the proposed SSM-P&O technique, it is related to the traditional P&O scheme. SS-P&O scheme results in the larger settling time (>1300 ms) and lower oscillations (0.05 rad/s). LS-P&O scheme results in larger oscillations (1.2 rad/s) and faster response (<77 ms), can affect the larger inertia machines. By employing modified P&O (MP&O) scheme [7], the settling time and oscillations can be controlled.

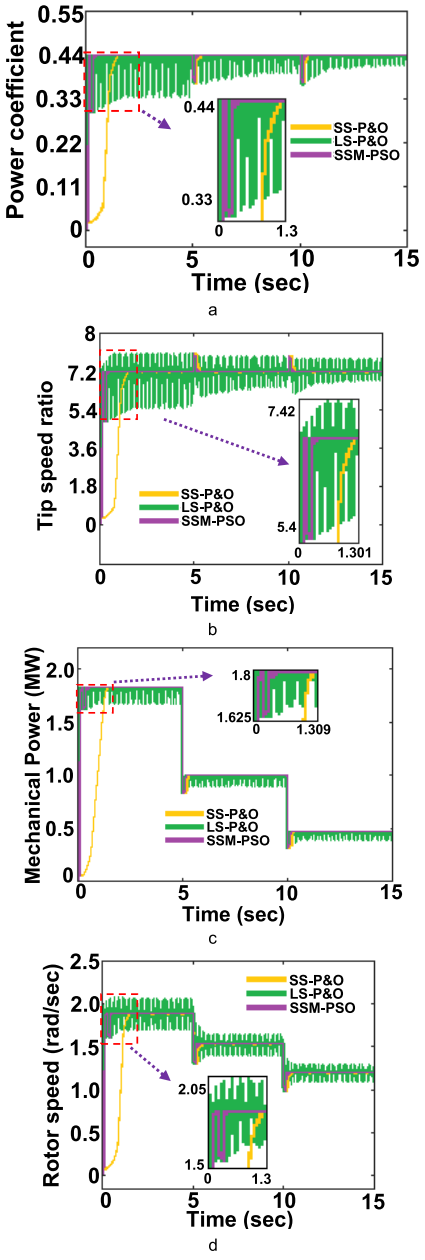

FIGURE 17. Rotor side characteristics for two step-down variation in wind speed (a) Power coefficient (b) Tip speed ratio (c) Mechanical power (d) Rotor speed.

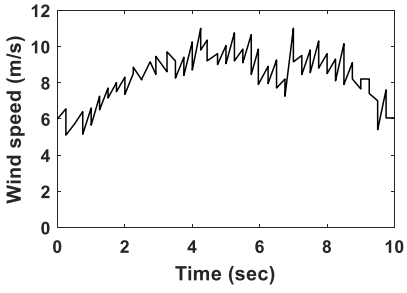

FIGURE 18. Random changes in wind-speed.

Even though in MP&O, settling time can be reduced to 930 ms, it displays a larger oscillation of 0.3 rad/s. The recently introduced robust adaptive step-sizes

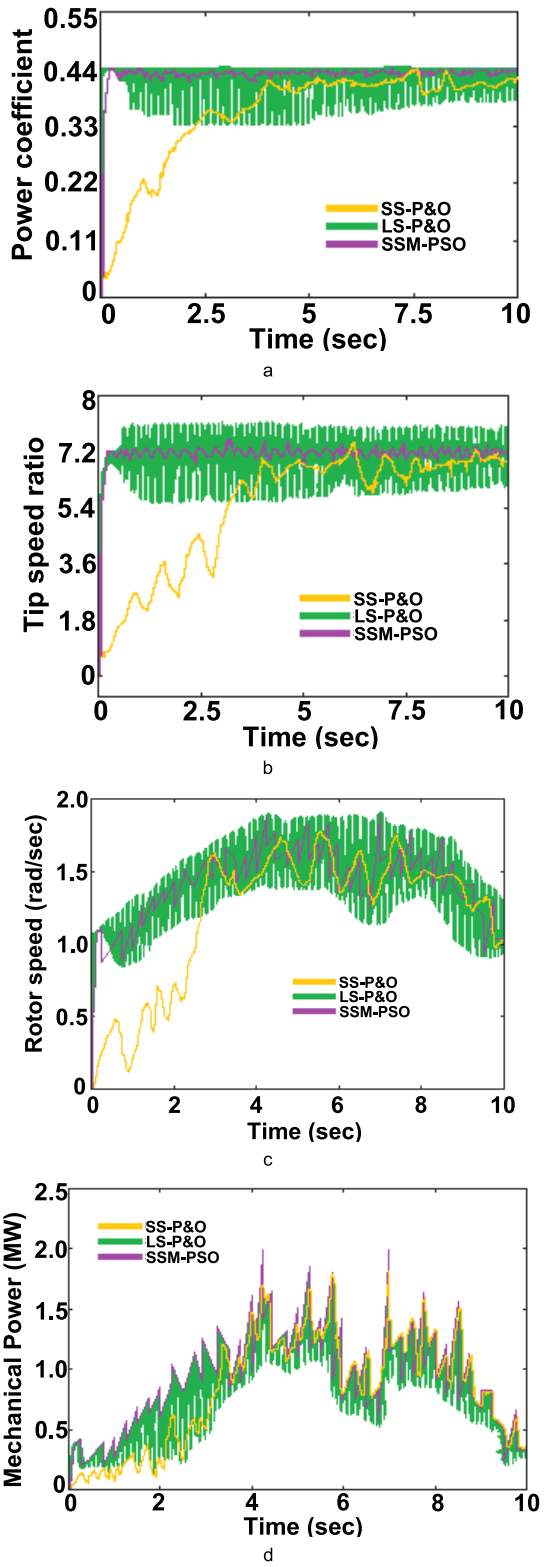

FIGURE 19. Rotor side characteristics for random variation in wind speed (a) Power coefficient (b) Tip speed ratio (c) Rotor speed (d) Mechanical power.

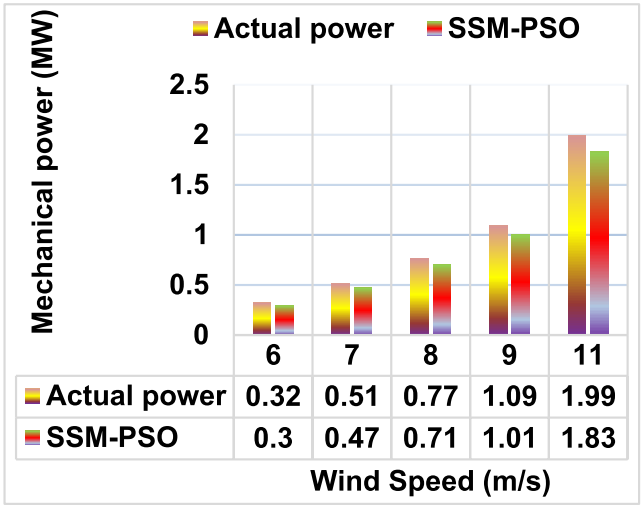

FIGURE 20. Efficiency of proposed SSM-PSO at different wind speeds.

P&O (RA-P&O) MPPT scheme in [7], displays the reduction in both settling time and oscillations to 600 ms and 0.001 rad/s, respectively. Moreover, the RA-P&O scheme displays an improvement in the tracking efficiency of 91.39%.

The proposed SSM-PSO scheme displays much lower settling time (<350 ms) compared to RA-P&O scheme. Also, the proposed SSM-PSO scheme results in the lesser oscillations of 0.001 rad/s. Moreover, the proposed SSM-PSO scheme displays an improved efficiency of 92.01%. Table-2 represents the comparison of the proposed SSM-PSO scheme with existing MPPT schemes, which also reflects the superiority of the SSM-PSO over other existing schemes.

VI. CONCLUSION

DFIG has the significant advantage of flexible operation at wide speed ranges. But, the non-linear $P-\omega$ characteristics result in the difficulty of tracking maximum power point. Already few conventional and optimization-based schemes are available in research platforms for tracking MPP. The optimization-based schemes avoid the oscillation behaviour over a steady state; same time, they result in more settling time. Compared with optimization-based schemes, conventional schemes are simpler and easily implementable in real-time situations. P&O method is the most generally employed conventional topology for tracking MPP. P&O method is normally operated with small and large step changes.

The P&O with smaller step-change results in the low oscillation of 0.05 rad/s over steady-state but results in the low tracking efficiency. Further, the P&O with large step changes results in lesser tracking of 77ms, but leads to higher oscillations. Since, the P&O is weather insensitive; it leads to fluctuation in output characteristics under a sudden change in wind speeds. The optimization-based schemes can avoid the -insensitive nature, but they result in complexity in execution during real-time.

PSO is the most commonly used and simply executable among existing optimization-based schemes. But, PSO results in a higher settling time, leading to a slower response. In this paper SSM-PSO scheme has been introduced to avoid the disadvantages of PSO. In the proposed

system, an anemometer has been employed to decide the space for placing particles in tracking MPP. The SSM-PSO scheme is successful in minimizing the searching space, leading to lesser MPP tracking time (<350ms). Also, the proposed SSM-PSO leads to the lesser oscillation of 0.001 rad/s. Moreover, the proposed SSM-PSO scheme is easily implementable due to its simple searching mechanism. The proposed SSM-PSO scheme has been implemented for 2MW DFIG system in MATLAB Simulink atmosphere, which displayed satisfactory results. The proposed work can be implemented using a hardware prototype as a future work.

ACKNOWLEDGMENT

The authors acknowledge the support given by the All India Council for Technical Education (AICTE), Department of Electrical and Communication Engineering, United Arab Emirates University, Al Ain, United Arab Emirates, and the National Water and Energy Center, UAE University.

REFERENCES

[1] H. Abu-Rub, M. Malinowski, and K. Al-Haddad, *Power Electronics for Renewable Energy Systems, Transportation and Industrial Applications*. Hoboken, NJ, USA: Wiley, 2014.
[2] A. Kasbi and A. Rahali, "Adaptive FOPI controller based on the fuzzy supervisory for wind power conversion system equipped by a doubly fed induction generator," *Int. Trans. Electr. Energy Syst.*, vol. 31, no. 8, Aug. 2021, Art. no. e12923, doi: 10.1002/2050-7038.12923.
[3] G. Abad, J. López, M. A. Rodríguez, L. Marroyo, and G. Iwanski, *Doubly Fed Induction Machine: Modeling and Control for Wind Energy Generation Applications*. Hoboken, NJ, USA: Wiley, 2011.
[4] N. Mendis, K. M. Muttaqi, S. Sayeef, and S. Perera, "Standalone operation of wind turbine-based variable speed generators with maximum power extraction capability," *IEEE Trans. Energy Convers.*, vol. 27, no. 4, pp. 822–834, Dec. 2012.
[5] K. S. Patel and V. H. Makwana, "Modified control technique of DFIG for power quality improvement," *IETE J. Educ.*, vol. 62, no. 1, pp. 44–54, 2021.
[6] F. Fateh, W. N. White, and D. Gruenbacher, "A maximum power tracking technique for grid-connected DFIG-based wind turbines," *IEEE J. Emerg. Sel. Topics Power Electron.*, vol. 3, no. 4, pp. 957–966, Dec. 2015.
[7] H. H. Mousa, A.-R. Youssef, and E. E. M. Mohamed, "Study of robust adaptive step-sizes P&O MPPT algorithm for high-inertia WT with direct-driven multiphase PMSG," *Int. Trans. Electr. Energy Syst.*, vol. 29, no. 10, 2019, Art. no. e12090, doi: 10.1002/2050-7038.12090.
[8] A. D. Falehi, "An innovative optimal RPO-FOSMC based on multi-objective grasshopper optimization algorithm for DFIG-based wind turbine to augment MPPT and FRT capabilities," *Chaos, Solitons Fractals*, vol. 130, Jan. 2020, Art. no. 109407.
[9] A.-R. Youssef, A. I. M. Ali, M. S. R. Saeed, and E. E. M. Mohamed, "Advanced multi-sector P&O maximum power point tracking technique for wind energy conversion system," *Int. J. Electr. Power Energy Syst.*, vol. 107, pp. 89–97, May 2019.
[10] J. Wang and D. Bo, "Adaptive fixed-time sensorless maximum power point tracking control scheme for DFIG wind energy conversion system," *Int. J. Electr. Power Energy Syst.*, vol. 135, Feb. 2022, Art. no. 107424.
[11] B. Yang, X. Zhang, T. Yu, H. Shu, and Z. Fang, "Grouped grey wolf optimizer for maximum power point tracking of doubly-fed induction generator based wind turbine," *Energy Convers. Manage.*, vol. 133, pp. 427–443, Feb. 2017.
[12] H. Chojaa, A. Derouich, S. E. Chehaidia, O. Zamzoum, M. Taoussi, and H. Elouatouat, "Integral sliding mode control for DFIG based WECS with MPPT based on artificial neural network under a real wind profile," *Energy Rep.*, vol. 7, pp. 4809–4824, Nov. 2021.
[13] K. Belmokhtar, M. L. Doumbia, and K. Agbossou, "Novel fuzzy logic based sensorless maximum power point tracking strategy for wind turbine systems driven DFIG (doubly-fed induction generator)," *Energy*, vol. 76, pp. 679–693, Nov. 2014.
[14] K. Han, T. Huang, and L. Yin, "Quantum parallel multi-layer Monte Carlo optimization algorithm for controller parameters optimization of doubly-fed induction generator-based wind turbines," *Appl. Soft Comput.*, vol. 112, Nov. 2021, Art. no. 107813.
[15] A. Fathy, A. G. Alharbi, S. Alshammari, and H. M. Hasanien, "Archimedes optimization algorithm based maximum power point tracker for wind energy generation system," *Ain Shams Eng. J.*, vol. 13, no. 2, Mar. 2022, Art. no. 101548.
[16] J. D. M. De Kooning, A. E. Samani, S. De Zutter, J. De Maeyer, and L. Vandevelde, "Techno-economic optimisation of small wind turbines using co-design on a parametrised model," *Sustain. Energy Technol. Assessments*, vol. 45, Jun. 2021, Art. no. 101165.
[17] M. M. Rezaei, "A nonlinear maximum power point tracking technique for DFIG-based wind energy conversion systems," *Eng. Sci. Technol., Int. J.*, vol. 21, no. 5, pp. 901–908, 2018.
[18] G. P. Prajapat, N. Senroy, and I. N. Kar, "Estimation based enhanced maximum energy extraction scheme for DFIG-wind turbine systems," *Sustain. Energy, Grids Netw.*, vol. 26, Jun. 2021, Art. no. 100419.
[19] Y. Sun, S. Yan, B. Cai, Y. Wu, and Z. Zhang, "MPPT adaptive controller of DC-based DFIG in resistances uncertainty," *Int. J. Control, Autom. Syst.*, vol. 19, no. 8, pp. 2734–2746, Aug. 2021.
[20] J. Kennedy and R. Eberhart, "Particle swarm optimization," in *Proc. Int. Conf. Neural Netw.*, Nov./Dec. 1995, pp. 1942–1948.
[21] S. Hassan, B. Abdelmajid, Z. Mourad, S. Aicha, and B. Abdennaceur, "PSO-backstepping controller of a grid connected DFIG based wind turbine," *Int. J. Electr. Comput. Eng.*, vol. 10, no. 1, pp. 856–867, Feb. 2020.
[22] M. Miyatake, M. Veerachary, F. Toriumi, N. Fujii, and H. Ko, "Maximum power point tracking of multiple photovoltaic arrays: A PSO approach," *IEEE Trans. Aerosp. Electron. Syst.*, vol. 47, no. 1, pp. 367–380, Jan. 2011.
[23] B. S. Goud, P. S. Varma, B. L. Rao, M. S. K. Reddy, A. Pandian, and C. R. Reddy, "Cuckoo search optimization based MPPT for integrated DFIG-wind energy system," in *Proc. IEEE Int. Conf. Decis. Aid Sci. Appl. (DASA)*, Nov. 2020, pp. 636–639.
[24] K. Ishaque, Z. Salam, M. Amjad, and S. Mekhilef, "An improved particle swarm optimization (PSO)–based MPPT for PV with reduced steady-state oscillation," *IEEE Trans. Power Electron.*, vol. 27, no. 8, pp. 3627–3638, Aug. 2012.
[25] K. Sundareswaran, P. Sankar, P. S. R. Nayak, S. P. Simon, and S. Palani, "Enhanced energy output from a PV system under partial shaded conditions through artificial bee colony," *IEEE Trans. Sustain. Energy*, vol. 6, no. 1, pp. 198–209, Jan. 2015.
[26] M. Seyedmahmoudian, S. Mekhilef, R. Rahmani, R. Yusof, and A. A. Shojaei, "Maximum power point tracking of partial shaded photovoltaic array using an evolutionary algorithm: A particle swarm optimization technique," *J. Renew. Sustain. Energy*, vol. 6, no. 2, Mar. 2014, Art. no. 023102.
[27] P. K. Gayen, D. Chatterjee, and S. K. Goswami, "Stator side active and reactive power control with improved rotor position and speed estimator of a grid connected DFIG (doubly-fed induction generator)," *Energy*, vol. 89, pp. 461–472, Sep. 2015.
[28] R. M. Linus and P. Damodharan, "Maximum power point tracking method using a modified perturb and observe algorithm for grid connected wind energy conversion systems," *IET Renew. Power Gener.*, vol. 9, no. 6, pp. 682–689, 2015.
[29] H. Fathabadi, "Novel highly accurate universal maximum power point tracker for maximum power extraction from hybrid fuel cell/photovoltaic/wind power generation systems," *Energy*, vol. 116, pp. 402–416, Dec. 2016.

BONI SATYA VARUN SAI received the M.Tech degree (Hons.) from JNTU Kakinada, Kakinada, India, in 2018. He is currently pursuing the Ph.D. degree in electrical engineering with Jadavpur University. His research interests includes photovoltaic cell modeling, MPPT schemes, and hybrid energy generation.

DEBASHIS CHATTERJEE received the M.E. degree from the Indian Institute of Technology Kharagpur, Kharagpur, India, in 1992, and the. Ph.D. degree from Jadavpur University, in 2005. Since 2012, he has been working as a Professor with Jadavpur University. His research interests includes speed sensor less control of induction motors, speed sensor less control of induction generators micro grid control, efficiency optimization of electric drive systems, electric vehicular drive development of solar/wind hybrid systems, and synchronization to grid.

SAAD MEKHILEF (Fellow, IEEE) is currently a Distinguished Professor at the School of Science, Computing and Engineering Technologies, Swinburne University of Technology, Australia, and an Honorary Professor at the Department of Electrical Engineering, University of Malaya. He has authored and co-authored more than 500 publications in academic journals and proceedings and five books with more than 34,000 citations, and more than 70 Ph.D. students graduated under his supervision. His research interests include power conversion techniques, control of power converters, maximum power point tracking (MPPT), renewable energy, and energy efficiency.

Prof. Mekhilef has been listed by Thomson Reuters (Clarivate Analytics) as one of the Highly Cited (World's Top 1%) engineering researchers in the world, in 2018, 2019, 2020, and 2021. He is actively involved in industrial consultancy for major corporations in the Power electronics and renewable energy projects. He is a fellow of IET. He serves as an Editorial Board Member for many top journals, such as IEEE TRANSACTION ON POWER ELECTRONICS, IEEE OPEN JOURNAL OF INDUSTRIAL ELECTRONICS, *IET Renewable Power Generation*, *Journal of Power Electronics*, and *International Journal of Circuit Theory and Applications*.

ADDY WAHYUDIE (Member, IEEE) received the B.S. degree in electrical engineering (majoring in control systems) from Gadjah Mada University, Indonesia, in 2002, the M.Eng. degree in electrical engineering from Chulalongkorn University, Thailand, in 2005, and the D.Eng. degree in electrical engineering from Kyushu University, Japan, in 2010. From 2005 to 2011, he was a Lecturer with the Department of Electrical Engineering, Gadjah Mada University. In 2011, he joined United Arab Emirates University, as an Assistant Professor, where he is currently an Associate Professor with the Department of Electrical Engineering. His research interests include control systems theory and its applications in electromechanical and renewable energy systems.